# Anisotropic optical trapping of ultracold erbium atoms

Maxence Lepers, J.-F. Wyart, Olivier Dulieu

# Anisotropic optical trapping of ultracold erbium atoms

M. Lepers,[1,*] J.-F. Wyart,[1,2] and O. Dulieu[1]

[1]*Laboratoire Aimé Cotton, UPR No. 3321 associée au CNRS, Université Paris–Sud, and ENS Cachan, Bâtiment 505, Campus d'Orsay, 91405 Orsay, France*

[2]*LERMA, UMR No. 8112, Observatoire de Paris–Meudon, Université Pierre et Marie Curie, 92195 Meudon, France*

(Received 23 October 2013; published 5 February 2014)

Ultracold atoms confined in a dipole trap are submitted to a potential whose depth is proportional to the real part of their dynamic dipole polarizability. The atoms also experience photon scattering whose rate is proportional to the imaginary part of their dynamic dipole polarizability. In this article we calculate the complex dynamic dipole polarizability of ground-state erbium, a rare-earth atom that was recently Bose condensed. The polarizability is calculated with the sum-over-state formula inherent to second-order perturbation theory. The summation is performed on transition energies and transition dipole moments from ground-state erbium, which are computed using the Racah-Slater least-squares fitting procedure provided by the COWAN codes. This allows us to predict nine unobserved odd-parity energy levels of total angular momentum $J = 5$, 6, and 7, in the range 25 000–31 000 cm$^{-1}$ above the ground state. Regarding the trapping potential, we find that ground-state erbium essentially behaves like a spherically symmetric atom, in spite of its large electronic angular momentum. We also find a mostly isotropic van der Waals interaction between two ground-state erbium atoms, characterized by a coefficient $C_6^{\rm iso} = 1760$ a.u. To the contrary, the photon-scattering rate shows a pronounced anisotropy since it strongly depends on the polarization of the trapping light.

DOI: 10.1103/PhysRevA.89.022505 PACS number(s): 31.15.ag, 31.15.ap, 32.10.Dk

## I. INTRODUCTION

In the field of ultracold atomic and molecular matter, quantum gases composed of particles with a strong intrinsic permanent dipole moment, referred to as dipolar gases, have attracted a great deal of interest over the past few years, as they can be manipulated by external electric or magnetic fields [1–4]. Due to the long-range and anisotropic particle-particle interactions, dipolar gases offer the possibility to produce and study highly correlated quantum matter, which is crucial for quantum information, or for the simulation of many-body or condensed-matter physics [5,6]. The production of ultracold heteronuclear bialkali molecules (which carry a permanent electric dipole moment in their own frame), in the ground electronic state [7,8], in the lowest rovibronic level [9,10], and even in the lowest hyperfine level [11] was a ground-breaking result, as it demonstrated the possibility to control both the internal and external molecular degrees of freedom [12].

Alternatively open-shell atoms possess a permanent magnetic dipole moment that is determined by their total angular momentum. The latter has the smallest possible nonzero value for alkali-metal atoms, namely, 1/2, but it can be significantly larger for transition-metal or rare-earth atoms. In the context of ultracold matter, the first Bose-Einstein condensates of highly magnetic atoms, obtained with chromium [13,14], were also crucial achievements. Later on, lanthanides started to draw much attention: Ultracold erbium atoms were produced in a magneto-optical trap [15,16]. More recently Bose-Einstein condensation was reached with erbium [17,18] and dysprosium [19–23] and noncondensed ultracold gases of thulium [24,25] and holmium [26] were also produced. These achievements stimulated both theoretical [27–31] and experimental studies [32–34], which complemented the work on ytterbium, the heavier (closed-shell) lanthanide element (see, for example, [35] and references therein).

In the present paper we investigate theoretically the optical trapping of ground-state $^3H_6$ erbium atoms. The efficiency of the trapping mechanism relies on the knowledge of the dynamic dipole polarizability, which is a complex quantity depending on the trapping laser frequency $\omega$ and determining the trapping potential depth and the photon-scattering rate. We compute the dynamic dipole polarizability with a sum-over-state formula, whose versatility enables us to calculate both the real and imaginary parts of the polarizability at any desired frequency. Two theoretical values of the static ($\omega = 0$) dipole polarizability have been reported in the literature [36,37], which were calculated with purely *ab initio* methods. However, as shown in recent papers, modeling lanthanides with such methods is a hard task. In the present work the relevant transition energies from the ground state and the related transition dipole moments are extracted from a semiempirical approach combining quantum-chemical calculations and experimental data. One central objective of this article is to determine to what extent the nonspherical electronic distribution of erbium induces an anisotropic response to the trapping light.

Unlike alkali-metal atoms, lanthanide atoms are characterized by a complex electronic structure with an open $4f$ and/or $5d$ subshells and a closed $6s$ shell. Since the electronic angular momentum associated with such configurations is large, the electronic distribution associated with a particular Zeeman sublevel is not spherically symmetric. In addition, the excitation of the core electrons occurring around 10 000 cm$^{-1}$ above the ground-state energy gives rise to very rich and complex spectra whose interpretation was an important contribution to atomic physics in the past four decades [38,39]. Today the knowledge of the spectroscopy of neutral and charged lanthanides including erbium is still incomplete [40–42]. Therefore, using the Racah-Slater least-squares fitting method implemented in the COWAN suite of codes [38],

*maxence.lepers@u-psud.fr

 

we adjust calculated and experimental energy levels. This allows us to give a revised theoretical interpretation of the spectrum of neutral erbium and to predict nine yet unobserved levels accessible from the ground state through electric dipole transition.

Since we manipulate a great deal of atomic data in this paper, it is necessary to label atomic levels precisely in addition to knowing their energy with respect to the ground state [43]. Strictly speaking, the only good quantum numbers are $J$, the total (orbital plus spin) angular momentum; $M_J$, its projection on a quantization axis $z$; and $p$, the parity. For particular states, e.g., the lowest states of erbium, the total orbital and spin angular momenta $L$ and $S$, respectively, are almost good quantum numbers. We also use the leading electronic configuration whose weight depends on the state under consideration (see the Appendix). For example, ground-state erbium is of even parity and its total angular momentum is $J = 6$. It is of $^3H$ character ($L = 5$, $S = 1$) up to 99%, the rest being $^1I$; its leading configuration is [Xe]$4f^{12}6s^2$. Since our calculations are mostly based on the Wigner-Eckart theorem, we will often label the atomic levels as $|\beta J M_J\rangle$, where $\beta$ stands for all quantum numbers but $J$ and $M_J$.

The paper is organized as follows. In Sec. II we give all the formulas necessary to characterize the optical trapping of non-spherically-symmetric atoms, in particular the potential depth and the photon-scattering rate induced by the trapping light. Section III is dedicated to the spectroscopy of erbium. We recall the main steps of the present approach based on the COWAN suite of codes and present our results for energies and transition dipole moments. In Sec. IV we report on our results and estimated accuracies for the polarizabilities of ground-state erbium. The reader interested in the final results is invited to go to Sec. IV C. Section V contains a summary and concluding remarks, emphasizing the van der Waals interactions between two erbium atoms determined here. More details on the atomic structure calculations are reported in the Appendix, including tables for fitting parameters used to model the erbium spectrum, energies, Landé factors, and configuration weights.

## II. OPTICAL TRAPPING OF NONSPHERICAL ATOMS

When spherically symmetric atoms, such as $^2S$ alkali-metal or $^1S$ alkaline-earth atoms, are submitted to an electromagnetic wave of angular frequency $\omega$ and intensity $I(\mathbf{r})$, with $\mathbf{r}$ the atomic center-of-mass position in the laboratory frame $xyz$ ($z$ being chosen as the quantization axis) they experience a potential energy [44] independent of the polarization of the field

$$U(\mathbf{r};\omega) = -\frac{1}{2\epsilon_0 c}\mathrm{Re}[\alpha_{\mathrm{scal}}(\omega)] \times I(\mathbf{r}), \tag{1}$$

which is due to the second-order ac Stark effect. In Eq. (1), $\alpha_{\mathrm{scal}}(\omega)$ is the (complex) scalar dynamic dipole polarizability of the atom, Re$[\cdots]$ denotes the real part, $\epsilon_0$ is the vacuum permittivity, and $c$ is the speed of light. The presence of the electromagnetic field also induces photon scattering with a rate equal to [44]

$$\Gamma(\mathbf{r};\omega) = \frac{1}{\hbar\epsilon_0 c}\mathrm{Im}[\alpha_{\mathrm{scal}}(\omega)] \times I(\mathbf{r}), \tag{2}$$

where Im$[\alpha_{\mathrm{scal}}(\omega)]$ is the imaginary part of the scalar dynamic dipole polarizability.

The complex polarizability is calculated by using the second-order time-dependent perturbation theory, which is cautiously discussed in Ref. [45], and by assigning to each excited level a complex energy $E_{\beta' J'} - i\hbar\gamma_{\beta' J'}/2$, $\gamma_{\beta' J'}$ being the inverse lifetime of the level $|\beta' J'\rangle$ [46]. This gives

$$\alpha_{\mathrm{scal}}(\omega) = \frac{1}{3(2J+1)}\sum_{\beta' J'}\left(\frac{|\langle\beta' J'\|d\|\beta J\rangle|^2}{E_{\beta' J'} - E_{\beta J} - i\frac{\hbar\gamma_{\beta' J'}}{2} - \hbar\omega} + \frac{|\langle\beta' J'\|d\|\beta J\rangle|^2}{E_{\beta' J'} - E_{\beta J} - i\frac{\hbar\gamma_{\beta' J'}}{2} + \hbar\omega}\right), \tag{3}$$

with $\langle\beta' J'\|d\|\beta J\rangle$ the reduced transition dipole moment. Then considering that the laser frequency is far from any atomic resonance, namely, $E_{\beta' J'} - E_{\beta J} - \hbar\omega \gg \hbar\gamma_{\beta' J'}/2$, and *a fortiori* $E_{\beta' J'} - E_{\beta J} + \hbar\omega \gg \hbar\gamma_{\beta' J'}/2$ since the atoms are in the ground state, we can separate real and imaginary parts

$$\mathrm{Re}[\alpha_{\mathrm{scal}}(\omega)] = \frac{2}{3(2J+1)}\sum_{\beta' J'}\frac{(E_{\beta' J'} - E_{\beta J})|\langle\beta' J'\|d\|\beta J\rangle|^2}{(E_{\beta' J'} - E_{\beta J})^2 - \hbar^2\omega^2}, \tag{4}$$

$$\mathrm{Im}[\alpha_{\mathrm{scal}}(\omega)] = \frac{1}{3(2J+1)}\sum_{\beta' J'}\frac{(E_{\beta' J'} - E_{\beta J})^2 + \hbar^2\omega^2}{[(E_{\beta' J'} - E_{\beta J})^2 - \hbar^2\omega^2]^2} \times \hbar\gamma_{\beta' J'}|\langle\beta' J'\|d\|\beta J\rangle|^2. \tag{5}$$

In contrast, the response of non-spherically-symmetric atoms such as erbium to an electromagnetic field depends on its polarization and on the magnetic sublevel $M_J$. In the general case of an elliptically polarized light with unit vector of polarization $\mathbf{e}$, the trapping potential equals [47]

$$U^{\mathrm{ell}}_{M_J}(\mathbf{r};\theta_p,\theta_k,\mathcal{A};\omega) = -\frac{1}{2\epsilon_0 c}I(\mathbf{r})\left\{\mathrm{Re}[\alpha_{\mathrm{scal}}(\omega)] + \mathcal{A}\cos\theta_k\frac{M_J}{2J}\mathrm{Re}[\alpha_{\mathrm{vect}}(\omega)] + \frac{3M_J^2 - J(J+1)}{J(2J-1)} \times \frac{3\cos^2\theta_p - 1}{2}\mathrm{Re}[\alpha_{\mathrm{tens}}(\omega)]\right\}, \tag{6}$$

where $\theta_p$ is such that $|\mathbf{e}\cdot\mathbf{e}_z|^2 = \cos^2\theta_p$, $\theta_k$ is the angle between $z$ and the wave vector $\mathbf{k}$, and $\mathcal{A}$ is the ellipticity parameter. Similarly to Eqs. (1) and (2), the photon-scattering rate $\Gamma^{\mathrm{ell}}_{M_J}$ is obtained by replacing Re$[\cdots]$ by Im$[\cdots]$ in Eq. (6). The quantities $\alpha_{\mathrm{vect}}(\omega)$ and $\alpha_{\mathrm{tens}}(\omega)$ are, respectively, the vector and tensor dynamic dipole polarizabilities, given by

$$\mathrm{Re}[\alpha_{\mathrm{vect}}(\omega)] = 2\sum_{\beta' J'}X^{(1)}_{JJ'}\frac{\hbar\omega|\langle\beta' J'\|d\|\beta J\rangle|^2}{(E_{\beta' J'} - E_{\beta J})^2 - \hbar^2\omega^2}, \tag{7}$$

$$\mathrm{Im}[\alpha_{\mathrm{vect}}(\omega)] = 2\sum_{\beta' J'}X^{(1)}_{JJ'}\frac{\hbar^2\omega\gamma_{\beta' J'}(E_{\beta' J'} - E_{\beta J})}{[(E_{\beta' J'} - E_{\beta J})^2 - \hbar^2\omega^2]^2} \times |\langle\beta' J'\|d\|\beta J\rangle|^2, \tag{8}$$

$$\mathrm{Re}[\alpha_{\mathrm{tens}}(\omega)] = 4\sum_{\beta' J'}X^{(2)}_{JJ'}\frac{(E_{\beta' J'} - E_{\beta J})|\langle\beta' J'\|d\|\beta J\rangle|^2}{(E_{\beta' J'} - E_{\beta J})^2 - \hbar^2\omega^2}, \tag{9}$$

$$\mathrm{Im}[\alpha_{\mathrm{tens}}(\omega)] = 2\sum_{\beta' J'} X^{(2)}_{JJ'} \frac{(E_{\beta' J'} - E_{\beta J})^2 + \hbar^2\omega^2}{[(E_{\beta' J'} - E_{\beta J})^2 - \hbar^2\omega^2]^2} \hbar\gamma_{\beta' J'} \times |\langle \beta' J' \| d \| \beta J \rangle|^2, \quad (10)$$

where $X^{(k)}_{JJ'}$ are angular factors [48]

$$X^{(1)}_{JJ'} = (-1)^{J+J'} \sqrt{\frac{6J}{(J+1)(2J+1)}} \begin{Bmatrix} 1 & 1 & 1 \\ J & J & J' \end{Bmatrix}, \quad (11)$$

$$X^{(2)}_{JJ'} = (-1)^{J+J'} \sqrt{\frac{5J(2J-1)}{6(J+1)(2J+1)(2J+3)}} \begin{Bmatrix} 1 & 1 & 2 \\ J & J & J' \end{Bmatrix}, \quad (12)$$

where the quantities in curly brackets are Wigner $6j$ symbols [49].

The particular case of a circular right (left) polarization is obtained by setting $\mathcal{A} = 1$ $(-1)$ in Eq. (6). For a linearly polarized field, corresponding to $\mathcal{A} = 0$, the trapping depends neither on the angle $\theta_k$ nor on the vector polarizability. In this case $\theta_p \equiv \theta$ is the angle between the polarization vector **e** and the quantization axis $z$. The trapping potential $U^{\mathrm{lin}}_{M_J}$ is obtained from Eq. (6),

$$U^{\mathrm{lin}}_{M_J}(\mathbf{r};\theta;\omega) = U^{\mathrm{ell}}_{M_J}(\mathbf{r};\theta_p \equiv \theta,\theta_k,\mathcal{A} = 0;\omega), \quad (13)$$

and similarly $\Gamma^{\mathrm{lin}}_{M_J}(\mathbf{r};\theta;\omega) = \Gamma^{\mathrm{ell}}_{M_J}(\mathbf{r};\theta_p \equiv \theta,\theta_k,\mathcal{A} = 0;\omega)$.

## III. THEORETICAL INTERPRETATION OF THE NEUTRAL ERBIUM SPECTRUM

Equations (4), (5), and (7)–(10) above show that the polarizabilities crucially depend on the transition energies and transition dipole moments from the erbium ground state. Therefore, the quality of those data as well as the method to calculate them represents a central issue of this work.

The initial steps that led to the critical compilation of erbium energy levels were summarized by Martin *et al.* [50] and later reported in [43]. After 1978, systematic studies of hyperfine effects in $4f^n5d6s6p$ configurations of neutral lanthanide atoms addressed the case of neutral erbium (Er I), but the fine-structure study preceding the determination of magnetic dipole and electric quadrupole parameters had to be limited to the terms of $4f^{11}5d6s6p$ arising from the ground term $^4I$ of the $4f^{11}$ core [51].

A first step in the description of Er I levels by means of the COWAN suite of codes [38] was used in an experimental determination of transition probabilities [42]. The COWAN codes led to energies and eigenfunctions by least-squares determination of radial parameters in appropriate sets of interacting electronic configurations, following the Racah-Slater method as recalled in [52]. The case of Er I turned out to be more complex than the one of singly ionized erbium (Er II) [40] because in neutral lanthanide atoms the lower levels of many excited configurations overlap the upper part of low-lying configurations. Before 1976, some levels with $7s$, $8s$, and $6d$ electrons were identified by means of very selective decays [from $4f^{12}6s(7s,8s,6d)$ to $4f^{12}6s6p$ and from $4f^{11}5d6s7s$ to $4f^{11}5d6s6p$] and of hazy emission line profiles that are common for such transitions in lanthanide atoms. The semiempirical designations were tabulated in [43,50]. Concerning configurations involving valence electrons, i.e., $5d$, $6s$, $6p$, and $6d$ electrons, estimates by Brewer [53,54] place the lowest levels of odd-parity configurations $4f^{12}5d6p$, $4f^{11}5d^3$, $4f^{11}6s6p^2$, and $4f^{13}6s$ in the energy range 37 000–43 000 cm$^{-1}$ above the ground level $4f^{12}6s^2\,{}^3H_6$. In the even-parity configurations, $4f^{11}5d^26p$, $4f^{12}6p^2$, and $4f^{12}5d^2$ should be present above $38\,500 \pm 2000$ cm$^{-1}$. Among those configurations that are still unobserved experimentally, the three with a $4f^{11}$ core generate 10 914 levels and the four others 1258 levels. Despite the progress of available computers since the earlier studies, the applicability of the parametric fitting in the Racah-Slater method is decreased when thousands of adjustable parameters are introduced by several tens of configurations. Therefore, we chose to restrict the number of electronic configurations included in the model. In the even-parity configurations, since we focus on the Er I ground state, we consider the lowest configuration $4f^{12}6s^2$. In the odd-parity configurations, we added the high-lying electronic configurations $4f^{12}5d6p$ and $4f^{13}6s$ to the known low-lying ones $4f^{11}5d6s^2$, $4f^{12}6s6p$, and $4f^{11}5d^26s$.

Let us briefly recall the principle of the calculations with the COWAN suite, which relies on four programs named RCN, RCN2, RCG, and RCE.

(i) First, for each configuration taken separately, the RCN program calculates the monoelectronic wave functions using the relativistic Hartree-Fock, usually referred to as HFR method. The wave functions are obtained by solving the Schrödinger equation, using a central-field potential describing electrostatic interactions and some relativistic corrections, i.e., mass-velocity, Darwin, and spin-orbit terms.

(ii) Then the RCN2 program calculates various radial integrals. For a given configuration, the direct and exchange Coulombic integrals $F^k(n\ell n'\ell')$ and $G^k(n\ell n'\ell')$ (for equivalent and nonequivalent electrons) and the spin-orbit energy $\zeta_{n\ell}$ for each subshell are computed. For each couple of configurations, the configuration-interaction Coulombic integrals $R^k(n\ell n'\ell',n''\ell''n'''\ell''')$ are evaluated. The radial integrals are treated in step (iv) as adjustable parameters.

(iii) Using those radial integrals, the RCG program diagonalizes the atomic Hamiltonian in an appropriate angular momentum basis, e.g., for a given value of $J$. From the resulting eigenenergies and eigenvectors, it models the atomic spectrum by calculating in particular the Einstein coefficients for all possible electric dipole transitions.

(iv) The energies calculated by RCG are then compared to the tabulated experimental levels. A fit of the atomic parameters is performed by the RCE program in order to minimize the mean error between experimental and theoretical energies. This produces a new set of parameters that serves as input for the final computation of the atomic spectrum by RCG [step (iii)].

It is important to stress that the basis functions used by the codes are the numerical functions obtained after the HFR calculation for each configuration, which are then appropriately combined to describe the atom in the desired angular momentum coupling scheme, i.e., $LS$, $jj$, or others. Note, finally, that we used both the McGuinness [55] and the Kramida [56] versions of COWAN codes.

The set of optimal atomic parameters that yields the input for the final call of RCG is given in the Appendix (see Tables IV and V). In the odd-parity configuration, $N_{\rm lev} = 208$ levels of the mixed configurations $4f^{11}5d6s^2$, $4f^{11}5d^26s$, and $4f^{12}6s6p$ are used to determine $N_{\rm par} = 24$ free parameters, 88 other parameters being constrained. The mean error is 65 cm$^{-1}$. The sizes of the basis sets are 525 for $J = 5$, 435 for $J = 6$, and 324 for $J = 7$. The results are listed in Tables VI and VII of the Appendix. The general agreement between experimental and theoretical Landé factors is a first indication of the quality of the eigenfunctions. The only noticeable exception is the inversion of the close $J = 5$ levels at 28 026 and 28 129 cm$^{-1}$. We also see nine theoretical levels that have not yet been observed experimentally. We predict those levels in a range of energy between 25 600 and 30 700 cm$^{-1}$ above the ground state, suggesting that they could be detected by direct transitions from the latter with current experimental devices [41,42].

## IV. CALCULATION OF ERBIUM POLARIZABILITIES

### A. Data sets of transition energies and dipole moments

The output of the previous calculations consists in a list of 1284 transition energies and Einstein coefficients from ground-state erbium. We call that list the data set T (after "theoretical"). From the Einstein coefficients, we can extract the squared reduced transition dipole moments necessary to compute the polarizabilities [see Eqs. (4), (5), and (7)–(10)], using the relation [38]

$$|\langle \beta' J' \| d \|^3 H_6 \rangle|^2 = \frac{3(2J'+1)\pi\epsilon_0\hbar^4 c^3 A_{\beta' J'}}{E^3_{\beta' J'}}, \qquad (14)$$

where $A_{\beta' J'}$ is the Einstein coefficient characterizing the transition between $|\beta' J'\rangle$ and the ground state and where the energy of the ground state has been set to zero.

We have seen in the previous section how the atomic parameters $F^k(n\ell n'\ell')$, $G^k(n\ell n'\ell')$, $\zeta_{n\ell}$, and $R^k(n\ell n'\ell', n''\ell'' n'''\ell''')$ have been adjusted to obtain the best possible agreement between theoretical and experimental energy levels. This adjustment is necessary to correct the defects of the HFR wave functions obtained with RCN. However, these wave functions are also used by RCN2 to calculate the monoelectronic radial matrix elements $\langle n'\ell'|\hat{r}|n\ell\rangle$, which are the building blocks of the Einstein coefficients computed by RCG. Therefore, a step of optimization of those radial matrix elements is also needed, which is the purpose of the present subsection.

We thus define the standard error on Einstein coefficients

$$\sigma = \left( \sum_{\beta' J'} \frac{\left(A^{\rm theor}_{\beta' J'} - A^{\rm expt}_{\beta' J'}\right)^2}{N_{\rm lev} - N_{\rm par}} \right)^{1/2}, \qquad (15)$$

where $N_{\rm lev}$ and $N_{\rm par}$ are the numbers of levels $|\beta' J'\rangle$ and adjusted parameters, respectively. We minimize $\sigma$ in Eq. (15) by varying the monoelectronic radial integrals $\langle n'\ell'|\hat{r}|n\ell\rangle$, thus introducing a scaling factor $f_{n\ell n'\ell'}$ (analogous to those defined in the Appendix)

$$\langle n'\ell'|\hat{r}|n\ell\rangle = f_{n\ell n'\ell'} \langle n'\ell'|\hat{r}|n\ell\rangle_{\rm HFR}, \qquad (16)$$

where $\langle n'\ell'|\hat{r}|n\ell\rangle_{\rm HFR}$ is the relativistic Hartree-Fock radial integral calculated by RCN2.

In order to compare theoretical and experimental Einstein coefficients, we consider the data set E (after "experimental") of the 33 transitions towards the erbium ground state, which was experimentally detected by Lawler *et al.* [42]. Moreover, we extract from the lines of the data set T those that have an experimental counterpart; this gives the data set T′. The scaling factors $f_{n\ell n'\ell'}$ are adjusted in order to obtain the best possible agreement between the Einstein coefficients of the data set T′ and E. Then the optimal scaling factors will be applied to the monoelectronic radial matrix elements composing the Einstein coefficients of data set T.

### B. Convergence and uncertainty

Now we discuss the convergence and reliability of our calculations, taking mostly the example of the real part of the scalar static dipole polarizability $\mathrm{Re}[\alpha_{\rm scal}(\omega = 0)]$ [see Eq. (4)]. This quantity is not relevant in the context of optical trapping, but there exist two theoretical values in the literature to which our results can be compared: 153 a.u. from Ref. [37] and 166 a.u. from Ref. [36]. The conclusions drawn for $\omega = 0$ can actually be extended to the first main resonances up to $\omega \simeq 20\,000$ cm$^{-1}$. Note that the imaginary part of the scalar static dipole polarizability will be examined separately.

#### 1. *Influence of data sets and scaling factors*

First, the influence of the different data sets with no adjustment on the scaling factors, i.e., $f_{n\ell n'\ell'} = 1$, is addressed (see the first three rows of Table I). The values obtained with the two theoretical data sets T and T′ clearly exceed the value obtained with the experimental data set E. To have better agreement between E and T′, we should use radial scaling factors smaller than unity. In addition, since for zero or small frequencies the scalar polarizability [Eq. (4)] is a sum of positive terms and since the set of experimental lines is *a priori* incomplete, the value from data set E (132 a.u.) can be regarded as the lower bound for $\alpha_{\rm scal}(0)$.

Given the configurations of odd parity that we include in our calculation of the erbium spectrum (see Sec. III), the transition-dipole-moment matrix elements involve two monoelectronic radial integrals: $\langle 4f|\hat{r}|5d\rangle$, coming from the transitions between the $4f^{12}6s^2$ and $4f^{11}5d6s$ configurations, and $\langle 6s|\hat{r}|6p\rangle$, coming from the transitions between the $4f^{12}6s^2$ and $4f^{12}6s6p$ configurations. We calculated the

TABLE I. Static scalar dipole polarizability $\mathrm{Re}[\alpha_{\rm scal}(\omega = 0)]$ for the different data sets and different scaling factors $f$ for the monoelectronic radial matrix elements (see the text). The number of levels $N_{\rm lev}$ of each data set is also indicated for the sake of clarity.

| Data set | $N_{\rm lev}$ | Scaling factor $f$ | $\mathrm{Re}[\alpha_{\rm scal}(0)]$ |
|---|---|---|---|
| E | 33 | | 132 |
| T′ | 33 | 1 | 200 |
| T | 1284 | 1 | 226 |
| T | 1284 | 0.81 | 148 |
| T | 1284 | 0.77 | 134 |

standard error on Einstein coefficients (15) between sets E and T′ and found that (i) it is much less sensitive to $f_{4f,5d}$ than to $f_{6s,6p}$ and (ii) the standard error is minimal ($\sigma = 1.36 \times 10^7$ s$^{-1}$ with $N_{\rm lev} = 33$ and $N_{\rm par} = 2$) for $f_{6s,6p} = 0.77$. Due to conclusion (i) we take identical scaling factors $f_{6s,6p} = f_{4f,5d} = f$ in what follows. The corresponding polarizability is 118 and 134 a.u. for data sets T′ and T, respectively. A closer look at the result shows that this scaling factor minimizes the error on the strongest line, whose upper level is the one of $J = 7$ at 24 943 cm$^{-1}$.

We made another test by searching the factor $f$ giving the same static dipole polarizability for the data sets T′ and E. We found $f = 0.81$ and a polarizability of 148 a.u. when applied to the set T. The two "optimal" scaling factors ($f = 0.77$ and 0.81) are rather close to each other. The difference can be explained because the second test allows for compensation effects between theoretical Einstein coefficients larger and smaller than the experimental ones.

In conclusion, we take the results obtained with the two previous tests, i.e., 134 a.u. with $f = 0.77$ and 148 a.u. with $f = 0.81$, as our lower and upper bounds of uncertainty and consider the mean value $f = 0.79$ as our optimal scaling factor. Therefore, we obtain $\mathrm{Re}[\alpha_{\rm scal}(\omega = 0)] = 141 \pm 7$ a.u., which is in good agreement with, although smaller than, the two literature values. It is important to stress that the uncertainty that we estimate here is only due to the calculation of the optimal scaling factor $f$. In particular, it does not take into account the uncertainty of the experimental results giving the data set E.

#### 2. Convergence on excited energy levels

Now that the question of scaling factors is solved, we discuss the convergence of the sum-over-state formulas inside the list of excited states in data set T. Namely, we truncate Eqs. (4), (5), (9), and (10) up to a given excited state $|N\rangle = |\beta_N J_N\rangle$ of energy $E_N$ and plot the resulting polarizabilities $\alpha^N_{\rm scal}(\omega = 0)$ and $\alpha^N_{\rm tens}(\omega = 0)$ as functions of $E_N$ [note that $\alpha_{\rm vect}(\omega = 0) = 0$].

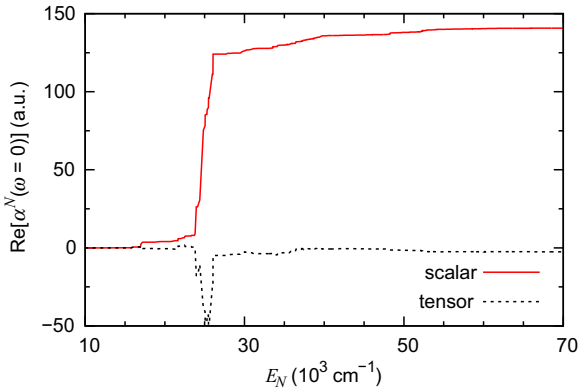


FIG. 1. (Color online) Convergence of the real part of the static scalar polarizability $\mathrm{Re}[\alpha^N_{\rm scal}(\omega = 0)]$ (solid line) and the static tensor polarizability $\mathrm{Re}[\alpha^N_{\rm tens}(\omega = 0)]$ (dotted line), with respect to the excited states of data set T. Equations (4) and (9) are truncated up to the excited state of energy $E_N$.

In Fig. 1 we focus on the real part of the scalar and tensor polarizabilities. We see that they are converged for $E_N \approx 60\,000$ cm$^{-1}$, where they reach at least 99% of their total value. In addition, the scalar polarizability reaches already 90% of its total value at $E_N \approx 30\,000$ cm$^{-1}$, that is, when the strongest lines have been included in the sum. In comparison, the lowest energies associated with configurations not included in our calculation are estimated around 40 000 cm$^{-1}$ above the ground state [53,54]. The convergence is visible on the tensor polarizability, although less spectacular, because the angular factor $X^{(2)}_{JJ'}$ [Eq. (12)] can change sign with $J'$. This fast convergence is due to the $(E_{\beta' J'} - E_{\beta J})^{-1}$ factor in Eq. (7), which enhances the importance of low-energy transitions; it is also inherent to the erbium spectrum, which is composed of a few strong lines among many weak lines.

#### 3. Imaginary part of the static scalar polarizability

In order to calculate the imaginary part of the polarizabilities, we need, in addition to transition energies and transition dipole moments, the lifetimes of all the excited states. Calculating the lifetime of a given state $|\beta' J'\rangle$ would require the Einstein coefficient of all the downward transitions from this state. Since we do not have this information here, we will rather make the assumption that all the excited states $|\beta' J'\rangle$ can only decay to the ground state. Within this approximation the inverse lifetime of the state $|\beta' J'\rangle$ is equal to the Einstein coefficient of the transition to the ground state

$$\gamma_{\beta' J'} \approx A_{\beta' J'}. \tag{17}$$

where $A_{\beta' J'}$ is given in Eq. (14).

We can check this hypothesis by calculating the imaginary part of the static polarizabilities with the data set E. Indeed, for the 33 transitions towards the erbium ground state reported in [42], the lifetime of the upper level was measured with the same device [41]. Therefore, we can calculate $\mathrm{Im}[\alpha_{\rm scal}(0)]$ using, on the one hand, the approximation (17) and, on the other hand, the measured lifetimes. We obtain very good agreement between the two methods, i.e., respectively, $\mathrm{Im}[\alpha_{\rm scal}(0)] = 1.42 \times 10^{-6}$ and $1.43 \times 10^{-6}$ a.u. $\mathrm{Im}[\alpha_{\rm tens}(0)] = -3.33 \times 10^{-7}$ and $-3.41 \times 10^{-7}$ a.u. (note that $\mathrm{Im}[\alpha_{\rm vect}(0)] = 0$). This result may seem surprising in view of the dense spectrum of erbium; however, it turns out that Eq. (17) is a very good approximation for the lowest excited states and the strongest transitions, present in data set E and which are prevailing for the imaginary part of the polarizabilities.

Figure 2 shows the imaginary part of the static polarizabilities as a function of $E_N$. For the sake of coherence we have used the same scaling factor $f = 0.79$ as for the real part of the polarizabilities. The convergence with $E_N$ is even faster than for the real part: At $E_N = 30\,000$ cm$^{-1}$, $\mathrm{Im}[\alpha^N_{\rm scal}(0)]$ and $\mathrm{Im}[\alpha^N_{\rm tens}(0)]$ differ by less than 1% from their final values given in Table II.

### C. Results

In order to present our results in a convenient way for experimental purposes, we give the polarizabilities of erbium in atomic units (units of $a_0^3$, with $a_0 = 0.052\,917\,721\,092$ nm the Bohr radius), but also the corresponding relevant quantities in physical units. The trapping potential (in temperature units

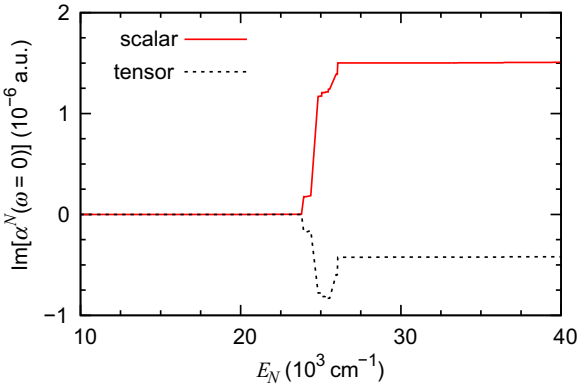


FIG. 2. (Color online) Convergence of the imaginary part of the scalar static polarizability $\mathrm{Im}[\alpha^N_{\mathrm{scal}}(\omega=0)]$ (solid line) and the static tensor polarizability $\mathrm{Im}[\alpha^N_{\mathrm{tens}}(\omega=0)]$ (dashed line), with respect to the excited states of data set T. Equations (5) and (10) are truncated up to the excited state of energy $E_N$.

K) corresponds to the real part of the polarizability (in a.u.)

$$U = \frac{2\pi a_0^3}{k_B c}\mathrm{Re}(\alpha) \times I \tag{18}$$

(with $I$ in W m$^{-2}$) and the photon-scattering rate (in s$^{-1}$) corresponds to the imaginary part of the polarizability (in a.u.)

$$\Gamma = \frac{4\pi a_0^3}{\hbar c}\mathrm{Im}(\alpha) \times I. \tag{19}$$

In what follows we assume an intensity of 1 GW m$^{-2}$, typical for a tight dipole trap (obtained for a laser power of 15 W and a Gaussian beam waist of 100 $\mu$m), which gives the potential (in $\mu$K GW$^{-1}$ m$^2$) $\overline{U} = 0.224\,946\,55 \times \mathrm{Re}(\alpha)$ and the rate (in s$^{-1}$ GW$^{-1}$ m$^2$) $\overline{\Gamma} = 5.890\,015\,5 \times 10^4 \times \mathrm{Im}(\alpha)$.

In Fig. 3 we plot the real part of the erbium polarizabilities and the corresponding trapping potentials as functions of the laser frequency (in cm$^{-1}$) and wavelength (in nm). We see a dense pattern of resonances for $\omega \geqslant 11\,000$ cm$^{-1}$, but most of them are narrow, which corresponds to weak transitions from the ground state, and the background profile of the polarizabilities is inherited from the strong lines. In Table II we focus on two frequencies: $\omega = 0$, to compare our results to the

TABLE II. Real and imaginary parts of the scalar, vector, and tensor dynamic dipole polarizabilities in atomic units, at $\omega = 0$ and 9398 cm$^{-1}$ ($\lambda = 1064$ nm), compared with available literature values.

| Polarizability \ $\omega$ (cm$^{-1}$) | 0 | 9398 |
|---|---|---|
| $\mathrm{Re}[\alpha_{\mathrm{scal}}(\omega)]$ | 141 | 164 |
| | 153 [37] | |
| | 166 [36] | |
| $\mathrm{Re}[\alpha_{\mathrm{vect}}(\omega)]$ | 0 | −0.943 |
| $\mathrm{Re}[\alpha_{\mathrm{tens}}(\omega)]$ | −2.52 | −3.93 |
| | −2.73 [36] | |
| $\mathrm{Im}[\alpha_{\mathrm{scal}}(\omega)]$ | $1.51 \times 10^{-6}$ | $2.34 \times 10^{-6}$ |
| $\mathrm{Im}[\alpha_{\mathrm{vect}}(\omega)]$ | 0 | $-1.74 \times 10^{-6}$ |
| $\mathrm{Im}[\alpha_{\mathrm{tens}}(\omega)]$ | $-4.21 \times 10^{-7}$ | $-6.90 \times 10^{-7}$ |

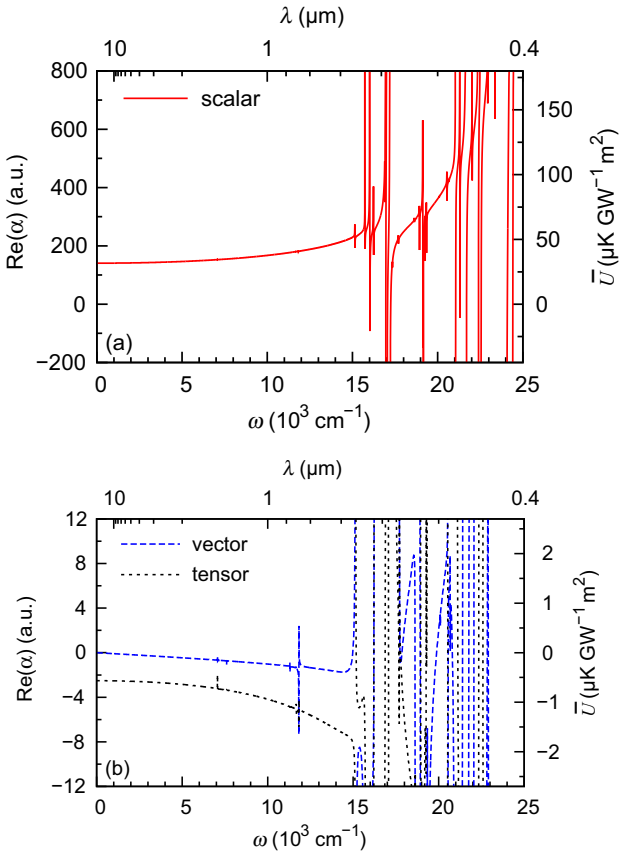


FIG. 3. (Color online) Real part of the (a) scalar and (b) vector and tensor (dashed and dotted lines, respectively) dynamic dipole polarizabilities in atomic units and corresponding trap depths obtained for an intensity of 1 GW m$^{-2}$, as functions of the trapping frequency $\omega$ (or wavelength $\lambda$).

literature, and $\omega = 9398$ cm$^{-1}$ ($\lambda = 1064$ nm), a widespread laser-trapping frequency, which is in the case of erbium far from any resonance. Our scalar and tensor polarizabilities are in good agreement, although smaller than the results from Refs. [36,37], which were calculated with purely *ab initio* methods.

The most striking feature, however, is that the vector and tensor contributions are found to be extremely small compared to the scalar contribution. This means that the trapping potential exerted on erbium atoms is almost isotropic, in the sense that it does not depend on the respective orientation of the electronic cloud and the light polarization. One possible explanation of that phenomenon is the following: The anisotropic response to the trapping light should be due to the electrons of the unfilled $4f$ shell; however, the latter is so contracted that the anisotropy is by far dominated by the isotropic response of the outermost $6s$ electrons.

The situation is drastically different for the imaginary part, for which the scalar, vector, and tensor polarizabilities are of the same order of magnitude (see Fig. 4 and Table II). The corresponding scaled photon-scattering rates are $\sim 0.1$ s$^{-1}$ GW$^{-1}$ m$^2$. After a cycle of absorption and spontaneous emission, a fraction of the atoms are too hot to be kept in the trap. Therefore, the atomic lifetime in the trap will strongly

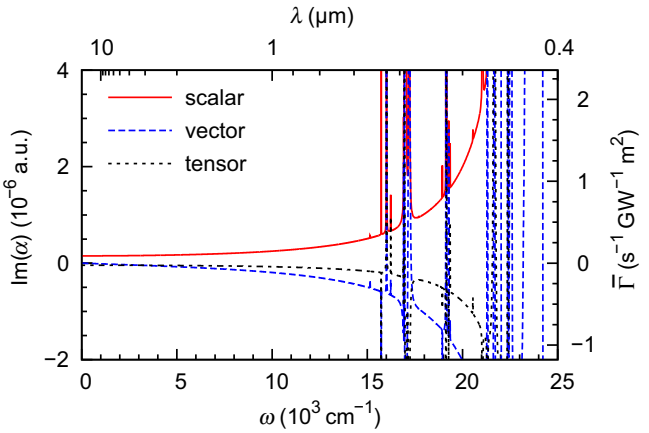


FIG. 4. (Color online) Imaginary part of the scalar, vector, and tensor dynamic dipole polarizabilities (solid, dashed, and dotted lines, respectively) in atomic units and corresponding photon-scattering rates obtained for an intensity of 1 GW m$^{-2}$, as functions of the trapping frequency $\omega$ (or wavelength $\lambda$).

depend on the orientation between the electronic and the light polarization. This is illustrated in Fig. 5, where the reduced photon-scattering rate $\bar{\Gamma}^{\rm lin}_{-J}$ for the lowest Zeeman sublevel

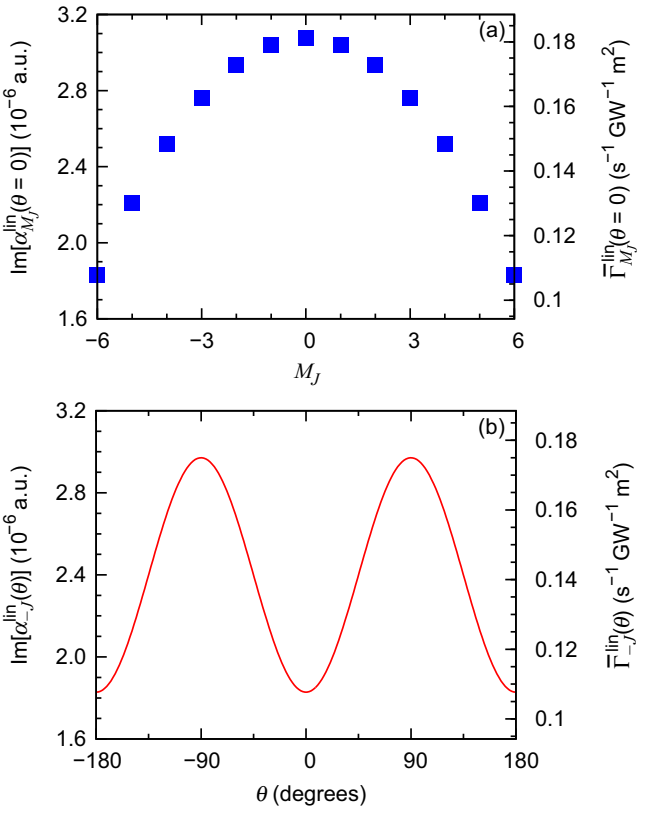


FIG. 5. (Color online) Imaginary part of the dynamic dipole polarizability in atomic units and corresponding photon-scattering rates obtained for a 1-GW m$^{-2}$ linearly polarized 1064-nm trapping light [see Eq. (2)]: (a) polarization axis parallel to the quantization axis ($\theta = 0^\circ$) as a function of the Zeeman sublevel $M_J$ and (b) the lowest sublevel $M_J = -J$ as a function of $\theta$.

is plotted as a function of the angle $\theta$ between the linearly polarized electric field and the quantization axis (given by an external magnetic field). Due to the negative sign of Im($\alpha_{\rm tens}$) the rate is the smallest, and so the trap is the most stable, in the collinear configuration ($\theta = 0^\circ$ or $180^\circ$). Similar behavior is observed as a function of $M_J$ for a fixed angle $\theta = 0^\circ$.

## V. CONCLUSION

In this article we gave a theoretical interpretation of the spectrum of neutral erbium that enables us to characterize the optical trapping of ultracold erbium atoms. We predicted nine unobserved levels that are accessible from the ground state through electric dipole transition. We obtained a list of transition energies and transition dipole moments that we used to calculate the real and imaginary parts of the scalar, vector, and tensor contributions to the ground-state polarizability. Although erbium is a non-spherically-symmetric atom, we showed that the trapping potential exerted by an infrared laser is essentially isotropic in the sense that it depends neither on the light polarization nor on the atomic Zeeman sublevel. In contrast, the photon-scattering rate exhibits a strong anisotropic behavior since the vector and tensor contributions to the imaginary part of the polarizability are of the same order of magnitude as the scalar contribution. We stressed that calculations made with different data sets of transition energies and dipole moments, including experimental ones, yield the same trends for trapping potential and photon-scattering rate.

The anisotropy of the photon-scattering rate opens the possibility to control the heating or the losses in the trap with an appropriate light polarization. The dependence of the photon-scattering rate on the atomic sublevel also results in different trap lifetimes for different Feshbach molecular states of $Er_2$, which are a current subject of interest [34].

Our calculations of polarizabilities are also relevant to characterize the long-range interactions between two erbium atoms. For nonpolarized atoms, i.e., not in a given Zeeman sublevel, the isotropic van der Waals coefficient $C_6^{\rm iso}$ can be calculated using the London formula $C_6^{\rm iso} = -(3/\pi)\int_0^{+\infty} d\omega\, {\rm Re}[\alpha_{\rm scal}(i\omega)]^2$, where $\alpha_{\rm scal}(i\omega)$ is the scalar polarizability at imaginary frequency, which gives for ground-state erbium $C_6^{\rm iso} = 1760$ a.u. In the case of polarized atoms, the $C_6$ coefficients also have an anisotropic contribution, which is very weak compared to the isotropic one since it is proportional to $\int_0^{+\infty} d\omega\, {\rm Re}[\alpha_{\rm scal}(i\omega)]{\rm Re}[\alpha_{\rm tens}(i\omega)] = -16.6$ a.u. and to $\int_0^{+\infty} d\omega\, {\rm Re}[\alpha_{\rm tens}(i\omega)]^2 = 0.265$ a.u. The $C_6$ coefficients between two polarized $^3H_6$ erbium atoms thus range from 1741 to 1766 a.u. depending on the molecular symmetry $|\Omega|_g$,$|\Omega|_u$,$0_g^+$ or $0_u^-$ of the $Er_2$ diatomic molecule, where $\Omega$ is the projection of the total angular momentum of the molecule on the internuclear axis. We display in Table III the minimal and maximal values of the $C_6$ coefficients induced by the anisotropy for the set of molecular states of a given symmetry. The variation is similar to the one obtained for dysprosium atoms [57]. Since the $C_6$ coefficients scale as the square of the dipole polarizabilities, their uncertainty due to scaling factors can be estimated as twice that of the polarizabilities, that is, 10%.

Knowledge of the polarizabilities of excited states and in particular of so-called magic frequencies or wavelengths,

TABLE III. Minimal and maximal values of the $C_6$ coefficients and number of molecular states for given symmetries $|\Omega|_g$,$|\Omega|_u$,$0_g^+$ or $0_u^-$ of the $Er_2$ diatomic molecule. Note that there is only one $C_6$ coefficient in the $12_g$ symmetry.

| Symmetry | Number of states | Min. $C_6$ | Max. $C_6$ |
|---|---|---|---|
| $0_g{}^+$,$0_u{}^-$ | 13 | 1741 | 1767 |
| $1_g$,$1_u$ | 24 | 1745 | 1766 |
| $2_g$,$2_u$ | 22 | 1748 | 1766 |
| $3_g$,$3_u$ | 20 | 1750 | 1765 |
| $4_g$,$4_u$ | 18 | 1752 | 1764 |
| $5_g$,$5_u$ | 16 | 1753 | 1762 |
| $6_g$,$6_u$ | 14 | 1754 | 1760 |
| $7_g$,$7_u$ | 12 | 1753 | 1758 |
| $8_g$,$8_u$ | 10 | 1752 | 1755 |
| $9_g$,$9_u$ | 8 | 1750 | 1752 |
| $10_g$,$10_u$ | 6 | 1748 | 1749 |
| $11_g$,$11_u$ | 4 | 1745 | 1745 |
| $12_g$ | 2 | 1741 | |

i.e., the wavelengths for which polarizabilities of the ground state and of a given excited state are equal, is of strong importance for precision measurements [58–60]. In Ref. [28], the authors calculate magic wavelengths for dysprosium atoms in a nonpolarized light. In the case of a polarized light, our preliminary calculations show that the anisotropy of trapping potential for erbium excited states tends to be larger than for the ground state. For example, at $\lambda = 1064$ nm the polarizabilities of the level $J = 7$ at 15 847 $cm^{-1}$ are $\mathrm{Re}(\alpha_{scal}) \approx 130$ a.u. and $\mathrm{Re}(\alpha_{scal}) \approx -60$ a.u. Thus, for the $M_J = -7$ sublevel in a linearly polarized electric field, $\mathrm{Re}(\alpha_{M_J=-7})$ varies from 70 a.u. for $\theta = 0°$ to 160 a.u. for $\theta = 90°$ [see Eq. (13)]. This opens the possibility of better control of the trapping conditions by tuning both the laser wavelength and the polarization angle, as recently shown for diatomic molecules [61].

## ACKNOWLEDGMENTS

Enlightening discussions with the members of the experimental team of Francesca Ferlaino in Innsbruck, in particular Kiyotaka Aikawa, Simon Baier, Albert Frisch, and Michael Mark, are gratefully acknowledged. M.L. is grateful to Eliane Luc for her guidance in theory of atomic structure. J.-F.W. acknowledges Laboratoire Aimé Cotton for its hospitality. Laboratoire Aimé Cotton is a member of Institut Francilien de Recherche sur les Atomes Froids.

## APPENDIX: DETAILS OF THE ATOMIC-STRUCTURE CALCULATIONS

This Appendix gives details of the calculation of the erbium atomic spectrum. Tables IV and V contain the optimal set of atomic parameters used for the last call of the diagonalization program RCG. For a given atomic parameter $P$, we multiply the HFR value by a scaling factor $\mathcal{F}_s(P)$ to obtain the input for the first call of RCG. The scaling factors $\mathcal{F}_s(P)$ given in Table IV and V were taken from the recent work on Er II [40]. In addition to $E_{av}$, $F^k(n\ell n\ell')$, $G^k(n\ell n\ell')$, $\zeta_{n\ell}$, and $R^k(n\ell n'\ell',n''\ell''n'''\ell''')$, the presence of effective parameters accounts for second-order configuration-interaction effects of far configurations. As explained in [38,39], those parameters are $\alpha$, $\beta$, and $\gamma$ for the configurations $4f^{11}$ and $4f^{12}$ and Slater-forbidden parameters $F^1(4f,5d)$, $G^2(4f,5d)$, and $G^4(4f,5d)$ for the configurations with open $4f$ and $5d$ subshells. Due to the lack of HFR evaluations, initial values for effective parameters are derived from semiempirical comparisons with similar spectra. Finally, Tables VI and VII contain the characteristics of the calculated even- and odd-parity levels of Er I, respectively.

TABLE IV. Fitted one-configuration parameters (in $cm^{-1}$) for odd-parity configurations of Er I compared with HFR radial integrals. The scaling factors are $\mathcal{F}_s(P) = P_{fit}/P_{HFR}$, except for $E_{av}$, when they are $P_{fit} - P_{HFR}$. The HFR values of $E_{av}$ parameters are relative to the ground-state configuration $4f^{12}6s^2$ taken as zero. Some parameters are constrained to vary in a constant ratio $r_n$, indicated in the second column, except if "fix" appears in the second or in the "Uncertainty" columns. In this case, the parameter $P$ is not adjusted. The columns for the uncertainty present the standard error of each parameter after the fitting procedure.

| Parameter $P$ | Constraint | $P_{fit}$ | Uncertainty | $P_{HFR}$ | $\mathcal{F}_s$ | $P_{fit}$ | Uncertainty | $P_{HFR}$ | $\mathcal{F}_s$ |
|---|---|---|---|---|---|---|---|---|---|
| | | $4f^{11}5d6s^2$ | | | | $4f^{11}5d^26s$ | | | |
| $E_{av}$ | | 46389 | 68 | 6742 | 39647 | 65582 | 74 | 23334 | 42248 |
| | | Fitted parameters | | | | Fitted parameters | | | |
| $F^2(4f4f)$ | $r_1$ | 97984 | 387 | 128939 | 0.760 | 97812 | 387 | 128712 | 0.760 |
| $F^4(4f4f)$ | $r_2$ | 69490 | 308 | 80847 | 0.860 | 69360 | 307 | 80696 | 0.860 |
| $F^6(4f4f)$ | $r_3$ | 49446 | 631 | 58150 | 0.850 | 49351 | 630 | 58039 | 0.850 |
| $\alpha$ | $r_4$ | 21.0 | 2 | | | 21.0 | 2 | | |
| $\beta$ | fix | −650 | | | | −650 | | | |
| $\gamma$ | fix | 2000 | | | | 2000 | | | |
| $F^2(5d5d)$ | | | | | | 21541 | 323 | 32674 | 0.659 |
| $F^4(5d5d)$ | | | | | | 16590 | 611 | 20683 | 0.802 |
| $\zeta_{4f}$ | $r_5$ | 2381 | 4 | 2428 | 0.981 | 2379 | 4 | 2426 | 0.981 |
| $\zeta_{5d}$ | $r_6$ | 803 | 9 | 948 | 0.847 | 665 | 7 | 785 | 0.847 |
| $F^1(4f5d)$ | $r_7$ | 671 | 70 | | | 671 | 70 | | |
| $F^2(4f5d)$ | $r_8$ | 15594 | 246 | 20265 | 0.770 | 13496 | 213 | 17539 | 0.769 |
| $F^4(4f5d)$ | $r_9$ | 10737 | 353 | 9189 | 1.168 | 9123 | 300 | 7807 | 1.169 |

TABLE IV. (*Continued*.)

| Parameter $P$ | Constraint | $P_{\text{fit}}$ | Uncertainty | $P_{\text{HFR}}$ | $\mathcal{F}_s$ | $P_{\text{fit}}$ | Uncertainty | $P_{\text{HFR}}$ | $\mathcal{F}_s$ |
|---|---|---|---|---|---|---|---|---|---|
| $G^1(4f5d)$ | $r_{10}$ | 4997 | 121 | 8711 | 0.574 | 4277 | 104 | 7456 | 0.574 |
| $G^2(4f5d)$ | $r_{11}$ | 1238 | 291 | | | 1238 | 291 | | |
| $G^3(4f5d)$ | $r_{12}$ | 6103 | 286 | 6893 | 0.885 | 5170 | 242 | 5840 | 0.885 |
| $G^4(4f5d)$ | $r_{13}$ | 1353 | 470 | | | 1353 | 470 | | |
| $G^5(4f5d)$ | $r_{14}$ | 4034 | 278 | 5204 | 0.775 | 3406 | 235 | 4394 | 0.775 |
| $G^3(4f6s)$ | $r_{15}$ | | | | | 1080 | 90 | 1486 | 0.727 |
| $G^2(5d6s)$ | $r_{17}$ | | | | | 12159 | 246 | 19202 | 0.633 |
| | | $4f^{12}6s6p$ | | | | $4f^{12}5d6p$ | | | |
| $E_{\text{av}}$ | | 36314 | 24 | 15491 | 20823 | 61570 | fix | 38570 | 23000 |
| $F^2(4f4f)$ | $r_1$ | 92534 | 366 | 121767 | 0.760 | 92314 | 365 | 121473 | 0.760 |
| $F^4(4f4f)$ | $r_2$ | 65336 | 290 | 76015 | 0.860 | 65168 | 289 | 75822 | 0.860 |
| $F^6(4f4f)$ | $r_3$ | 46412 | 592 | 54582 | 0.850 | 46294 | 591 | 54441 | 0.850 |
| $\alpha$ | $r_4$ | 21.0 | 2 | | | 21.0 | 2 | | |
| $\beta$ | fix | −650 | | | | −650 | | | |
| $\gamma$ | fix | 2000 | | | | 2000 | | | |
| $\zeta_{4f}$ | $r_5$ | 2242 | 4 | 2286 | 0.981 | 2242 | 4 | 2284 | 0.981 |
| $\zeta_{5d}$ | $r_6$ | | | | | 463 | 5 | 547 | 0.846 |
| $\zeta_{6p}$ | $r_{18}$ | 1496 | 18 | 1035 | 1.445 | 1107 | 13 | 766 | 1.445 |
| $F^1(4f5d)$ | $r_7$ | | | | | 671 | 70 | | |
| $F^2(4f5d)$ | $r_8$ | | | | | 11010 | 174 | 14308 | 0.703 |
| $F^4(4f5d)$ | $r_9$ | | | | | 7345 | 241 | 6286 | 1.168 |
| $F^1(4f6p)$ | fix | 100 | | | | 150 | | | |
| $F^2(4f6p)$ | $r_{19}$ | 3698 | 155 | 3267 | 1.13 | 2943 | 123 | 2610 | 1.13 |
| $F^2(6p5d)$ | fix | | | | | 11470 | | 14438 | 0.80 |
| $G^1(4f5d)$ | fix | | | | | 3898 | | 6652 | 0.724 |
| $G^2(4f5d)$ | fix | | | | | 1092 | | | |
| $G^3(4f5d)$ | fix | | | 9357 | 0.898 | 4397 | | 4913 | 0.895 |
| $G^4(4f5d)$ | fix | | | | | 1028 | | | |
| $G^5(4f5d)$ | fix | | | | | 2761 | | 3625 | 0.762 |
| $G^3(4f6s)$ | $r_{15}$ | 1210 | 101 | 1665 | 0.727 | | | | |
| $G^2(4f6p)$ | $r_{19}$ | 843 | 35 | 748 | 1.13 | 643 | | 568 | 1.13 |
| $G^4(4f6p)$ | $r_{19}$ | 733 | 31 | 650 | 1.13 | 556 | | 491 | 1.13 |
| $G^1(6s6p)$ | | 12843 | 66 | 23373 | 0.549 | | | | |
| $G^1(6p5d)$ | fix | | | | | 7880 | | 13133 | 0.60 |
| $G^3(6p5d)$ | fix | | | | | 5052 | | 8420 | 0.60 |

TABLE V. Same as Table IV for configuration-interaction parameters.

| Parameter $P$ | Constraint | $P_{\text{fit}}$ | Uncertainty | $P_{\text{HFR}}$ | $\mathcal{F}_s$ |
|---|---|---|---|---|---|
| | | $4f^{11}5d6s^2$-$4f^{11}5d^26s$ | | | |
| $R^2(4f6s,4f5d)$ | fix | −710 | | −938 | 0.757 |
| $R^3(4f6s,4f5d)$ | fix | 1002 | | 770 | 0.757 |
| $R^2(5d6s,5d5d)$ | $r_{17}$ | −13919 | 282 | −21982 | 0.633 |
| | | $4f^{11}5d6s^2$-$4f^{12}6s6p$ | | | |
| $R^1(5d6s,4f6p)$ | $r_{20}$ | −3163 | 96 | −6878 | 0.46 |
| $R^3(5d6s,6p4f)$ | $r_{20}$ | −678 | 21 | −1474 | 0.46 |
| | | $4f^{11}5d^26s$-$4f^{12}6s6p$ | | | |
| $R^1(5d5d,4f6p)$ | fix | 2813 | | 3715 | 0.757 |
| $R^3(5d5d,4f6p)$ | fix | 753 | | 994 | 0.757 |
| | | $4f^{11}5d^26s$-$4f^{12}5d6p$ | | | |
| $R^1(5d6s,4f6p)$ | fix | −2966 | | −5932 | 0.5 |
| $R^3(5d6s,4f6p)$ | fix | −660 | | −1320 | 0.5 |

TABLE VI. Comparison of energies $E$ and Landé factors $g_L$ of Er I even-parity levels. The superscript "expt" stands for experimental values that are taken from [50]. The superscript "theor" stands for the theoretical values from the present parametric calculations. Note that $\Delta E = E^{\text{expt}} - E^{\text{theor}}$.

| Configuration | Term | $J$ | $E^{\text{expt}}$ | $g_L^{\text{expt}}$ | $\Delta E$ | $g_L^{\text{theor}}$ |
|---|---|---|---|---|---|---|
| $4f^{12}6s^2$ | $^3H$ | 6 | 0 | 1.16381 | −9 | 1.166 |
| $4f^{12}6s^2$ | $^3F$ | 4 | 5035.193 | 1.147 | 49 | 1.141 |
| $4f^{12}6s^2$ | $^3H$ | 5 | 6958.329 | 1.031 | −15 | 1.033 |
| $4f^{12}6s^2$ | $^3H$ | 4 | 10750.982 | 0.936 | −116 | 0.945 |
| $4f^{12}6s^2$ | $^3F$ | 3 | 12377.534 | 1.065 | −53 | 1.084 |
| $4f^{12}6s^2$ | $^3F$ | 2 | 13097.906 | 0.750 | 25 | 0.739 |

TABLE VII. Same as Table VI for Er I odd-parity levels with electric dipole decay to the ground level. The theoretical values $E^{\text{theor}}$, the factors $g_L^{\text{theor}}$, and the percentage of calculated configurations are derived by means of the RCG code with the parameter set reported in Table IV. In the configuration notations, $A$ stands for $4f^{12}$, $B$ for $4f^{11}$, $ds^2$ for $5d6s^2$, $sp$ for $6s6p$, $d^2s$ for $5d^26s$, and $dp$ for $5d6p$. The lowercase letters or arabic numbers appearing in the seventh column correspond to different intermediate coupling schemes [38].

| | | | | | Leading electronic | % leading $LS$-coupling | Configuration weight (%) | | | |
|---|---|---|---|---|---|---|---|---|---|---|
| $E^{\text{expt}}$ [50] | $E^{\text{theor}}$ | $\Delta E$ | $g_L^{\text{expt}}$ | $g_L^{\text{theor}}$ | configuration | component | $B$-$ds^2$ | $B$-$d^2s$ | $A$-$sp$ | $A$-$dp$ |
| | | | | | $J = 5$ | | | | | |
| 11401.197 | 11419.6 | −18 | 1.205 | 1.210 | $B$-$ds^2$ | 51 $B$–$ds^2(^4I)\,^5G$ | 97.5 | 2.3 | 0.3 | 0 |
| 15185.352 | 15258.6 | −7 | 1.160 | 1.170 | $B$-$ds^2$ | 55 $B$–$ds^2(^4I)\,^3G$ | 96.7 | 2.3 | 1.0 | 0 |
| 17029.058 | 17023.5 | 6 | 1.150 | 1.136 | $B$-$ds^2$ | 37 $B$–$ds^2(^4I)\,^5H$ | 97.3 | 2.3 | 0.3 | 0 |
| 17347.860 | 17314.6 | 33 | 1.175 | 1.177 | $A$-$sp$ | 33 $A$–$sp(^3H)\,^3Ga$ | 0.3 | 1.2 | 98.1 | 0.4 |
| 19201.343 | 19250.1 | −49 | 1.060 | 1.059 | $A$-$sp$ | 25 $A$–$sp(^3H)\,^1H$ | 16.2 | 0.9 | 82.6 | 0.3 |
| 19563.116 | 19383.6 | 180 | 0.990 | 0.990 | $B$-$ds^2$ | 26 $B$–$ds^2(^4I)\,^5I$ | 81.1 | 2.1 | 16.8 | 0.1 |
| 20917.276 | 20790.1 | 127 | 0.980 | 0.980 | $B$-$ds^2$ | 23 $B$–$ds^2(^4I)\,^5K$ | 97.6 | 2.2 | 0.2 | 0 |
| 21392.817 | 21419.2 | −26 | 1.005 | 1.019 | $B$-$ds^2$ | 18 $B$–$ds^2(^4I)\,^3I$ | 95.6 | 2.6 | 1.7 | 0.1 |
| 22124.268 | 22136.3 | −12 | 1.285 | 1.264 | $A$-$sp$ | 28 $A$–$sp(^3F)\,^5F$ | 0.3 | 15.6 | 83.7 | 0.4 |
| 22450.111 | 22571.5 | −121 | 1.360 | 1.370 | $B$-$d^2s$ | 35 $B$–$d^2s(^4I)\,^7F$ | 1.4 | 82.7 | 15.8 | 0.1 |
| 22672.766 | 22651.3 | 21 | 1.040 | 1.040 | $B$-$ds^2$ | 22 $B$–$ds^2(^4I)\,^5K$ | 92.0 | 3.7 | 4.0 | 0.2 |
| 23447.079 | 23475.0 | −28 | 1.080 | 1.084 | $A$-$sp$ | 23 $A$–$sp(^3H)\,^5I$ | 1.0 | 1.9 | 96.8 | 0.4 |
| 23855.654 | 23878.9 | −23 | 1.140 | 1.178 | $A$-$sp$ | 26 $A$–$sp(^3F)\,^5F$ | 1.7 | 1.9 | 96.0 | 0.4 |
| 23885.406 | 23903.7 | −18 | 1.100 | 1.058 | $A$-$sp$ | 22 $A$–$sp(^3H)\,^5I$ | 4.6 | 1.7 | 93.3 | 0.5 |
| 24083.166 | 24055.6 | 28 | 1.128 | 1.132 | $A$-$sp$ | 46 $A$–$sp(^3H)\,^3Gb$ | 37.1 | 1.7 | 58.5 | 2.6 |
| 25162.553 | 25170.9 | −8 | 1.010 | 1.016 | $B$-$ds^2$ | 24 $B$–$ds^2(^4I)\,^3I$ | 74.9 | 3.5 | 20.5 | 1.1 |
| 25364.012 | 25382.3 | −18 | 1.180 | 1.183 | $B$-$d^2s$ | 13 $B$–$d^2s(^4I)\,^7Ha$ | 1.6 | 96.8 | 1.4 | 3.2 |
| 25681.933 | 25598.0 | 84 | 1.175 | 1.142 | $B$-$ds^2$ | 20 $B$–$ds^2(^4F)\,^5F$ | 81.1 | 3.0 | 15.0 | 0.9 |
| 26198.837 | 26145.5 | 53 | 1.045 | 1.069 | $A$-$sp$ | 48 $A$–$sp(^3H)\,^5H$ | 0.1 | 1.4 | 98.1 | 0.3 |
| | 27651.7 | | | 1.315 | $B$-$d^2s$ | 41 $B$–$d^2s(^4I)\,^5Fb$ | 2.2 | 97.0 | 0.8 | 0.1 |
| 27856.436 | 27825.9 | 31 | 1.095 | 1.145 | $B$-$d^2s$ | 15 $B$–$d^2s(^4I)\,^7G$ | 8.0 | 87.7 | 4.1 | 0.2 |
| 28026.045 | 28090.7 | −65 | 1.120 | 1.056 | $A$-$sp$ | 18 $A$–$sp(^3H)\,^5I$ | 12.7 | 9.4 | 77.5 | 0.4 |
| 28129.803 | 28141.9 | −12 | 1.040 | 1.125 | $B$-$ds^2$ | 10 $B$–$ds^2(^4G)\,^5G$ | 67.6 | 8.6 | 23.6 | 0.3 |
| 29272.207 | 29237.0 | 35 | 1.115 | 1.123 | $B$-$ds^2$ | 37 $B$–$ds^2(^4F)v^5H$ | 95.1 | 2.7 | 2.1 | 0.1 |
| 29550.807 | 29770.5 | −220 | 1.150 | 1.168 | $B$-$ds^2$ | 32 $B$–$ds^2(^4F)\,^5G$ | 69.7 | 4.6 | 25.0 | 0.7 |
| 29794.862 | 29821.6 | −27 | 1.100 | 1.131 | $A$-$sp$ | 14 $A$–$sp(^3F)\,^5F$ | 17.1 | 4.5 | 78.1 | 0.3 |
| 29894.203 | 30064.0 | −170 | 1.195 | 1.126 | $B$-$d^2s$ | 17 $B$–$d^2s(^4I)\,^7Ia$ | 1.8 | 90.5 | 7.3 | 0.4 |
| 30380.282 | 30326.8 | 53 | 1.116 | | $A$-$sp$ | 20 $A$–$sp(^3F)\,^3Gb$ | 15.6 | 27.3 | 53.9 | 3.3 |
| 30600.160 | 30768.9 | −169 | 1.195 | 1.093 | $B$-$d^2s$ | 8 $B$–$d^2s(^4I)\,^5Hc$ | 4.9 | 78.4 | 15.2 | 1.4 |
| 31105.090 | 30988.2 | 117 | 1.200 | 1.250 | $B$-$d^2s$ | 37 $B$–$d^2s(^4I)\,^5Fa$ | 0.6 | 96.4 | 2.1 | 0.9 |
| 31194.235 | 31185.2 | 9 | 1.135 | 1.128 | $B$-$ds^2$ | 16 $B$–$ds^2(^4F)\,^5H$ | 86.5 | 9.5 | 3.8 | 0.2 |
| 31364.719 | 31360.7 | 4 | 1.235 | 1.232 | $A$-$sp$ | 4 $A$–$sp(^3F)\,^5G$ | 2.5 | 5.1 | 92.1 | 0.4 |
| 31442.927 | 31475.4 | −33 | 1.195 | 1.132 | $B$-$d^2s$ | 12 $B$–$d^2s(^4I)\,^5Fa$ | 3.7 | 90.5 | 5.2 | 0.6 |
| | | | | | $J = 6$ | | | | | |
| 7176.503 | 7185.5 | −9 | 1.302 | 1.304 | $B$-$ds^2$ | 77 $B$–$ds^2(^4I)\,^5G$ | 98.2 | 1.8 | 0 | 0 |
| 11799.778 | 11788.5 | 11 | 1.190 | 1.195 | $B$-$ds^2$ | 39 $B$–$ds^2(^4I)\,^5H$ | 96.9 | 2.5 | 0.5 | 0 |

TABLE VII. (*Continued.*)

| $E^{\text{expt}}$ [50] | $E^{\text{theor}}$ | $\Delta E$ | $g_L^{\text{expt}}$ | $g_L^{\text{theor}}$ | Leading electronic configuration | % leading $LS$-coupling component | Configuration weight (%) $B$-$ds^2$ | $B$-$d^2s$ | $A$-$sp$ | $A$-$dp$ |
|---|---|---|---|---|---|---|---|---|---|---|
| 16070.095 | 16125.4 | −55 | 1.200 | 1.169 | $B$-$ds^2$ | 42 $B$–$ds^2(^4I)\,^3H$ | 76.5 | 2.3 | 19.1 | 0.2 |
| 16321.110 | 16347.4 | −26 | 1.220 | 1.254 | $A$-$sp$ | 59 $A$–$sp(^3H)\,^5G$ | 14.6 | 1.4 | 83.7 | 0.3 |
| 17073.800 | 17063.7 | 10 | 1.070 | 1.069 | $A$-$sp$ | 27 $A$–$sp(^3H)\,^3Ia$ | 2.9 | 1.1 | 95.6 | 0.4 |
| 17456.383 | 17461.9 | −6 | 1.070 | 1.058 | $B$-$ds^2$ | 23 $B$–$ds^2(^4I)\,^5I$ | 96.5 | 2.7 | 0.8 | 0 |
| 19326.598 | 19273.3 | 53 | 1.180 | 1.175 | $A$-$sp$ | 31 $A$–$sp(^3H)\,^5H$ | 0.5 | 0.8 | 98.3 | 0.3 |
| 19508.432 | 19461.5 | 47 | 0.960 | 0.960 | $B$-$ds^2$ | 35 $B$–$ds^2(^4I)\,^5K$ | 96.7 | 2.5 | 0.8 | 0 |
| 20166.130 | 20213.2 | −47 | 1.485 | 1.475 | $B$-$d^2s$ | 78 $B$–$d^2s(^4I)\,^7F$ | 0.1 | 99.9 | 0 | 0 |
| 20737.723 | 20659.6 | 78 | 0.855 | 0.853 | $B$-$ds^2$ | 49 $B$–$ds^2(^4I)\,^5L$ | 97.6 | 2.3 | 0.2 | 0 |
| 21701.885 | 21786.2 | −84 | 1.055 | 1.045 | $B$-$ds^2$ | 25 $B$–$ds^2(^4I)\,^3I$ | 91.3 | 2.9 | 5.5 | 0.2 |
| 22583.504 | 22501.1 | 82 | 1.130 | 1.137 | $B$-$ds^2$ | 36 $B$–$ds^2(^4F)\,^5G$ | 95.6 | 2.5 | 1.8 | 0.1 |
| 23311.577 | 23311.6 | 0 | 1.250 | 1.267 | $B$-$d^2s$ | 22 $B$–$d^2s(^4I)\,^7Ha$ | 0.4 | 97.3 | 2.3 | 0.1 |
| 23831.359 | 23820.4 | 11 | 1.250 | 1.248 | $A$-$sp$ | 56 $A$–$sp(^3F)\,^5G$ | 0.3 | 2.9 | 96.4 | 0.4 |
| 24246.146 | 24215.8 | 30 | 1.085 | 1.098 | $A$-$sp$ | 43 $A$–$sp(^3H)\,^5I$ | 1.3 | 1.6 | 96.7 | 0.4 |
| 24457.139 | 24492.3 | −35 | 1.050 | 1.054 | $B$-$ds^2$ | 24 $B$–$ds^2(^4F)\,^3H$ | 84.4 | 2.7 | 12.3 | 0.6 |
| 25268.259 | 25308.9 | −40 | 1.185 | 1.166 | $B$-$d^2s$ | 17 $B$–$d^2s(^4I)\,^7G$ | 6.3 | 91.8 | 1.7 | 0.1 |
| 25392.779 | 25419.3 | −27 | 1.075 | 1.072 | $B$-$ds^2$ | 21 $B$–$ds^2(^4F)\,^5G$ | 82.9 | 9.3 | 7.4 | 0.4 |
| 25880.274 | 26070.5 | −190 | 1.150 | 1.156 | $A$-$sp$ | 41 $A$–$sp(^3H)\,^3Hb$ | 19.9 | 2.3 | 75.7 | 2.1 |
| 26237.004 | 26178.0 | 59 | 1.160 | 1.158 | $A$-$sp$ | 36 $A$–$sp(^3H)\,^3Ha$ | 15.3 | 2.7 | 80.1 | 1.9 |
| 27582.017 | 27490.5 | 91 | 1.120 | 1.113 | $B$-$d^2s$ | 12 $B$–$d^2s(^4I)\,^5Ha$ | 0.5 | 98.9 | 0.4 | 0.2 |
| 27879.416 | 27996.0 | −117 | 1.175 | 1.147 | $B$-$ds^2$ | 23 $B$–$ds^2(^4G)\,^5G$ | 90.0 | 7.9 | 2.0 | 0.1 |
| 28854.941 | 28902.8 | −48 | 1.190 | 1.208 | $B$-$d^2s$ | 22 $B$–$d^2s(^4I)\,^5Gb$ | 3.1 | 96.0 | 0.8 | 0.1 |
| 29152.796 | 29118.8 | 34 | 1.175 | 1.192 | $B$-$d^2s$ | 15 $B$–$d^2s(^4I)\,^7Hb$ | 0.6 | 99.0 | 0.1 | 0.2 |
| 29561.425 | 29584.5 | −24 | 1.130 | 1.126 | $A$-$sp$ | 25 $A$–$sp(^3F)\,^5G$ | 0.2 | 3.1 | 96.2 | 0.4 |
| | 29718.1 | | | 1.114 | $B$-$d^2s$ | 9 $B$–$d^2s(^4I)\,^3Ic$ | 16.1 | 81.3 | 2.3 | 0.3 |
| 30007.369 | 30051.0 | −44 | 1.090 | 1.092 | $B$-$ds^2$ | 14 $B$–$ds^2(^2H)\,^1I2$ | 67.8 | 31.2 | 0.9 | 0.1 |
| 30088.200 | 30169.1 | −81 | 1.120 | 1.126 | $B$-$d^2s$ | 17 $B$–$d^2s(^4I)\,^7Ka$ | 12.1 | 87.3 | 0.4 | 0.2 |
| | 30702.6 | | | 1.268 | $B$-$d^2s$ | 26 $B$–$d^2s(^4I)\,^5Ga$ | 1.6 | 97.6 | 0.3 | 0.4 |
| 30765.720 | 30771.7 | −6 | 1.205 | 1.205 | $B$-$ds^2$ | 51 $B$–$ds^2(^4F)\,^5H$ | 95.6 | 4.4 | 0.1 | 0 |
| 31205.223 | 31264.5 | −59 | 1.100 | 1.090 | $B$-$d^2s$ | 14 $B$–$d^2s(^4I)\,^7Ia$ | 0.6 | 99.1 | 0.1 | 0.2 |
| 31823.748 | 31706.0 | 118 | 1.045 | 1.078 | $A$-$sp$ | 39 $A$–$sp(^3H)\,^3Ib$ | 6.7 | 27.7 | 61.9 | 3.7 |
| 31926.003 | 31939.5 | −13 | 1.215 | 1.215 | $B$-$d^2s$ | 18 $B$–$d^2s(^4I)\,^5Gd$ | 4.1 | 76.4 | 18.0 | 1.5 |
| | | | | | $J = 7$ | | | | | |
| 7696.956 | 7713.9 | −17 | 1.266 | 1.262 | $B$-$ds^2$ | 78 $B$–$ds^2(^4I)\,^5H$ | 98.0 | 2.0 | 0 | 0 |
| 11887.503 | 11937.5 | −50 | 1.153 | 1.150 | $B$-$ds^2$ | 47 $B$–$ds^2(^4I)\,^3I$ | 96.6 | 2.9 | 0.5 | 0 |
| 15846.549 | 15844.1 | 2 | 1.070 | 1.066 | $B$-$ds^2$ | 43 $B$–$ds^2(^4I)\,^5K$ | 96.6 | 2.4 | 0.9 | 0 |
| 17157.307 | 17129.3 | 28 | 1.195 | 1.192 | $A$-$sp$ | 39 $A$–$sp(^3H)\,^5I$ | 1.9 | 1.1 | 96.6 | 0.4 |
| 17796.139 | 17809.4 | −13 | 1.110 | 1.107 | $B$-$ds^2$ | 48 $B$–$ds^2(^4I)\,^5I$ | 95.4 | 2.8 | 1.7 | 0.0 |
| 18774.123 | 18737.9 | 36 | 0.965 | 0.967 | $B$-$ds^2$ | 45 $B$–$ds^2(^4I)\,^5L$ | 97.6 | 2.4 | 0 | 0 |
| 19125.253 | 19052.2 | 73 | 1.235 | 1.244 | $A$-$sp$ | 68 $A$–$sp(^3H)\,^5H$ | 0 | 1.0 | 98.6 | 0.4 |
| 21168.430 | 21162.2 | 6 | 1.065 | 1.062 | $B$-$ds^2$ | 33 $B$–$ds^2(^4I)\,^3K$ | 95.9 | 2.9 | 1.1 | 0.1 |
| 21787.932 | 21749.2 | 39 | 1.350 | 1.360 | $B$-$d^2s$ | 49 $B$–$d^2s(^4I)\,^7G$ | 0.2 | 99.8 | 0 | 0 |
| 23080.952 | 23046.6 | 34 | 1.010 | 1.011 | $B$-$ds^2$ | 40 $B$–$ds^2(^4I)\,^3L$ | 97.0 | 2.8 | 0.2 | 0 |
| 23364.853 | 23396.3 | −31 | 1.225 | 1.226 | $B$-$d^2s$ | 24 $B$–$d^2s(^4I)\,^7G$ | 0.3 | 99.6 | 0.2 | 0 |
| 24943.272 | 24946.1 | −3 | 1.160 | 1.145 | $A$-$sp$ | 57 $A$–$sp(^3H)\,^3Ib$ | 3.9 | 6.5 | 84.6 | 4.9 |
| 25159.143 | 25167.9 | −9 | 1.170 | 1.170 | $B$-$d^2s$ | 12 $B$–$d^2s(^4I)\,^7Ha$ | 0.9 | 93.8 | 4.9 | 0.4 |
| 25598.286 | 25570.2 | 28 | 1.155 | 1.166 | $A$-$sp$ | 48 $A$–$sp(^3H)\,^5I$ | 0.4 | 2.0 | 97.1 | 0.5 |
| | 25659.2 | | | 1.146 | $B$-$ds^2$ | 48 $B$–$ds^2(^4F)\,^5H$ | 96.6 | 3.1 | 0.3 | 0 |
| 27230.646 | 27134.8 | 96 | 1.135 | 1.113 | $B$-$d^2s$ | 12 $B$–$d^2s(^4I)\,^1Ka$ | 0.2 | 99.5 | 0.1 | 0.2 |
| 27306.747 | 27432.5 | −126 | 1.225 | 1.243 | $B$-$d^2s$ | 25 $B$–$d^2s(^4I)\,^7Hb$ | 0.1 | 99.8 | 0 | 0.1 |
| 28017.584 | 28087.3 | −70 | 1.080 | 1.068 | $B$-$ds^2$ | 24 $B$–$ds^2(^2H)\,^3K2$ | 93.5 | 6.5 | 0 | 0 |
| | 28306.8 | | | 1.220 | $B$-$d^2s$ | 19 $B$–$d^2s(^4I)\,^7Hb$ | 1.8 | 98.0 | 0.1 | 0.1 |
| | 29088.0 | | | 1.171 | $B$-$d^2s$ | 18 $B$–$d^2s(^4I)\,^5Hb$ | 2.1 | 97.9 | 0 | 0 |
| | 29781.0 | | | 1.069 | $B$-$d^2s$ | 15 $B$–$d^2s(^4I)\,^1Kb$ | 1.8 | 98.0 | 0 | 0.2 |
| | 30127.6 | | | 1.215 | $B$-$d^2s$ | 21 $B$–$d^2s(^4I)\,^5Hf$ | 12.0 | 87.9 | 0.1 | 0.1 |
| | 30353.5 | | | 1.117 | $B$-$d^2s$ | 17 $B$–$ds^2(^2H)\,^3I2$ | 45.1 | 54.6 | 0.2 | 0.1 |

[1] L. D. Carr and J. Ye, New J. Phys. **11**, 055009 (2009).
[2] O. Dulieu and C. Gabbanini, Rep. Prog. Phys. **72**, 086401 (2009).
[3] M. A. Baranov, Phys. Rep. **464**, 71 (2008).
[4] T. Lahaye, C. Menotti, L. Santos, M. Lewenstein, and T. Pfau, Rep. Prog. Phys. **72**, 126401 (2009).
[5] I. Bloch, J. Dalibard, and S. Nascimbène, Nat. Phys. **8**, 267 (2012).
[6] V. Galitski and I. B. Spielman, Nature (London) **494**, 49 (2013).
[7] D. Wang, J. Qi, M. F. Stone, O. Nikolayeva, H. Wang, B. Hattaway, S. D. Gensemer, P. L. Gould, E. E. Eyler, and W. C. Stwalley, Phys. Rev. Lett. **93**, 243005 (2004).
[8] J. M. Sage, S. Sainis, T. Bergeman, and D. DeMille, Phys. Rev. Lett. **94**, 203001 (2005).
[9] K.-K. Ni, S. Ospelkaus, M. H. G. de Miranda, A. Peer, B. Neyenhuis, J. J. Zirbel, S. Kotochigova, P. S. Julienne, D. S. Jin, and J. Ye, Science **322**, 231 (2008).
[10] J. Deiglmayr, A. Grochola, M. Repp, K. Mörtlbauer, C. Glück, J. Lange, O. Dulieu, R. Wester, and M. Weidemüller, Phys. Rev. Lett. **101**, 133004 (2008).
[11] S. Ospelkaus, K.-K. Ni, G. Quéméner, B. Neyenhuis, D. Wang, M. H. G. de Miranda, J. L. Bohn, J. Ye, and D. S. Jin, Phys. Rev. Lett. **104**, 030402 (2010).
[12] M. H. G. de Miranda, A. Chotia, B. Neyenhuis, D. Wang, G. Quéméner, S. Ospelkaus, J. L. Bohn, J. Ye, and D. S. Jin, Nat. Phys. **7**, 502 (2011).
[13] A. Griesmaier, J. Werner, S. Hensler, J. Stuhler, and T. Pfau, Phys. Rev. Lett. **94**, 160401 (2005).
[14] Q. Beaufils, R. Chicireanu, T. Zanon, B. Laburthe-Tolra, E. Maréchal, L. Vernac, J.-C. Keller, and O. Gorceix, Phys. Rev. A **77**, 061601 (2008).
[15] H. Ban, M. Jacka, J. Hanssen, J. Reader, and J. McClelland, Opt. Express **13**, 3185 (2005).
[16] J. J. McClelland and J. L. Hanssen, Phys. Rev. Lett. **96**, 143005 (2006).
[17] A. Frisch, K. Aikawa, M. Mark, A. Rietzler, J. Schindler, E. Zupanič, R. Grimm, and F. Ferlaino, Phys. Rev. A **85**, 051401 (2012).
[18] K. Aikawa, A. Frisch, M. Mark, S. Baier, A. Rietzler, R. Grimm, and F. Ferlaino, Phys. Rev. Lett. **108**, 210401 (2012).
[19] M. Lu, S. H. Youn, and B. L. Lev, Phys. Rev. Lett. **104**, 063001 (2010).
[20] S. H. Youn, M. Lu, U. Ray, and B. L. Lev, Phys. Rev. A **82**, 043425 (2010).
[21] S. H. Youn, M. Lu, and B. L. Lev, Phys. Rev. A **82**, 043403 (2010).
[22] M. Lu, S. H. Youn, and B. L. Lev, Phys. Rev. A **83**, 012510 (2011).
[23] M. Lu, N. Q. Burdick, S. H. Youn, and B. L. Lev, Phys. Rev. Lett. **107**, 190401 (2011).
[24] D. Sukachev, A. Sokolov, K. Chebakov, A. Akimov, S. Kanorsky, N. Kolachevsky, and V. Sorokin, Phys. Rev. A **82**, 011405 (2010).
[25] D. Sukachev, K. Chebakov, A. Sokolov, A. Akimov, N. Kolachevsky, and V. Sorokin, Opt. Spectrosc. **111**, 633 (2011).
[26] J. Miao, J. Hostetter, G. Stratis, and M. Saffman, Bull. Am. Phys. Soc. (2013), http://meetings.aps.org/Meeting/DAMOP13/Session/U2.5.
[27] V. A. Dzuba and V. V. Flambaum, Phys. Rev. A **81**, 052515 (2010).
[28] V. A. Dzuba, V. V. Flambaum, and B. L. Lev, Phys. Rev. A **83**, 032502 (2011).
[29] M. Tomza, Phys. Rev. A **88**, 012519 (2013).
[30] A. Kozlov, V. A. Dzuba, and V. V. Flambaum, Phys. Rev. A **88**, 032509 (2013).
[31] U. I. Safronova, A. S. Safronova, and P. Beiersdorfer, Phys. Rev. A **88**, 032512 (2013).
[32] B. K. Newman, N. Brahms, Y. S. Au, C. Johnson, C. B. Connolly, J. M. Doyle, D. Kleppner, and T. J. Greytak, Phys. Rev. A **83**, 012713 (2011).
[33] A. Frisch, K. Aikawa, M. Mark, F. Ferlaino, E. Berseneva, and S. Kotochigova, Phys. Rev. A **88**, 032508 (2013).
[34] A. Frisch, M. Mark, K. Aikawa, F. Ferlaino, J. L. Bohn, C. Makrides, A. Petrov, and S. Kotochigova, arXiv:1312.1972.
[35] C. Cohen-Tannoudji and K. W. Madison, *Annual Review of Cold Atoms and Molecules* (World Scientific, Singapore, 2013), Chap. 1.
[36] X. Chu, A. Dalgarno, and G. C. Groenenboom, Phys. Rev. A **75**, 032723 (2007).
[37] D. R. Lide, *CRC Handbook of Chemistry and Physics* (CRC, Boca Raton, FL, 2012).
[38] R. D. Cowan, *The Theory of Atomic Structure and Spectra* (University of California Press, Berkeley, 1981).
[39] B. R. Judd, Rep. Prog. Phys. **48**, 907 (1985).
[40] J. F. Wyart and J. E. Lawler, Phys. Scr. **79**, 045301 (2009).
[41] E. A. Den Hartog, J. P. Chisholm, and J. E. Lawler, J. Phys. B **43**, 155004 (2010).
[42] J. E. Lawler, J. F. Wyart, and E. A. Den Hartog, J. Phys. B **43**, 235001 (2010).
[43] Yu. Ralchenko, A. E. Kramida, and J. Reader, NIST Atomic Spectra Database, version 3.1.5, 2009.
[44] R. Grimm, M. Weidemüller, and Y. B. Ovchinnikov, Adv. At. Mol. Opt. Phys. **42**, 95 (2000).
[45] P. W. Langhoff, S. T. Epstein, and M. Karplus, Rev. Mod. Phys. **44**, 602 (1972).
[46] R. Vexiau, N. Bouloufa, M. Aymar, J. G. Danzl, M. J. Mark, H. C. Nägerl, and O. Dulieu, Eur. Phys. J. D **65**, 243 (2011).
[47] N. L. Manakov, V. D. Ovsiannikov, and L. P. Rapoport, Phys. Rep. **141**, 320 (1986).
[48] J. R. P. Angel and P. G. H. Sandars, Proc. R. Soc. London Ser. A **305**, 125 (1968).
[49] D. A. Varshalovich, A. N. Moskalev, and V. K. Khersonskii, *Quantum Theory of Angular Momentum* (World Scientific, Singapore, 1988).
[50] W. C. Martin, R. Zalubas, and L. Hagan, *Atomic Energy Levels—The Rare Earth Elements, Natl. Bur. Stand. Ref. Data Ser., Natl. Bur. Stand. (US) Circ. No. 60* (US GPO, Washington, DC, 1978), p. 332.
[51] H. D. Kronfeldt, D. Ashkenasi, S. Kröger, and J. F. Wyart, Phys. Scr. **48**, 688 (1993).
[52] J. F. Wyart, Phys. Scr. **82**, 035302 (2010).
[53] L. Brewer, J. Opt. Soc. Am. **61**, 1666 (1971).
[54] L. Brewer, in *Systematics of the Properties of the Lanthanides*, edited by S. P. Sinha (Reidel, Dordrecht, 1983).
[55] C. McGuinness, Los Alamos version of the COWAN codes for Linux, 2009. Avaliable at http://www.tcd.ie/Physics/people/Cormac.McGuinness/Cowan/.
[56] A. Kramida, PC version of the COWAN codes, 2010. Avaliable at http://das101.isan.troitsk.ru/COWAN.

[57] S. Kotochigova and A. Petrov, Phys. Chem. Chem. Phys. **13**, 19165 (2011).

[58] S. G. Porsev, A. Derevianko, and E. N. Fortson, Phys. Rev. A **69**, 021403 (2004).

[59] M. Takamoto, F. L. Hong, R. Higashi, and H. Katori, Nature (London) **435**, 321 (2005).

[60] A. D. Ludlow, T. Zelevinsky, G. K. Campbell, S. Blatt, M. M. Boyd, M. H. G. De Miranda, M. J. Martin, J. W. Thomsen, S. M. Foreman, J. Ye *et al*., Science **319**, 1805 (2008).

[61] B. Neyenhuis, B. Yan, S. A. Moses, J. P. Covey, A. Chotia, A. Petrov, S. Kotochigova, J. Ye, and D. S. Jin, Phys. Rev. Lett. **109**, 230403 (2012).